

A Self-Consistent Model for High Repetition Rate Copper Vapor Lasers

M. J. KUSHNER

Abstract—A computer model for a high repetition rate copper vapor laser is described. Equations for the discharge pulse, laser pulse, and interpulse afterglow period are simultaneously integrated over many discharge cycles until a consistent solution is obtained. In this way, consistent initial conditions are obtained and many scaling characteristics of the copper laser are successfully reproduced. This is a major improvement over models which consider only a single-laser pulse. By modeling both an ideal and real laser, and comparing the results to experimental data, we have determined that the peak electron temperature and the initial density of metastable copper are the factors which dominate the performance of the laser. Processes which effect these two quantities are therefore the most important in describing the laser.

I. INTRODUCTION

HIGH repetition rate (HRR) electric discharge metal vapor lasers are a practical source of high peak and high average power in the visible. The copper laser (5106 and 5782 Å) has, in particular, been the object of an intense development program in this country as well as in Israel and Russia [1]–[3]. More than 100 W from a single oscillator and hundreds of watts from a multichain oscillator-amplifier arrangement have been reported [4]. The most sophisticated HRR copper lasers are resonantly charged electric discharge devices. These lasers are self heated; the energy required to heat the laser tube and vaporize the copper comes from the discharge itself. For a given repetition rate, buffer gas pressure, and discharge pulse energy ($\frac{1}{2} CV^2$), insulation surrounding the discharge tube determines the tube temperature and hence copper vapor pressure.

The copper laser is a cyclic or self terminating laser. The upper laser level is resonant to the ground state while the lower laser level is metastable. Thus, atoms making the laser transition accumulate in the lower level and eventually cause the gain to become negative. Since oscillation cannot be achieved if the density of copper atoms in the lower level is too large at the beginning of the discharge pulse, the slow collisional relaxation rate of the lower level sets an upper limit on the repetition rate. Thus, the choice of repetition rate immediately sets threshold pumping requirements; that is, the number of atoms which must be excited to the upper level in order to reach threshold. The choice of repetition rate also determines the initial conditions for the discharge pulse since the initial electron density (i.e., plasma tube impedance) and electron temperature are a function of interpulse processes.

Previously reported models of the copper vapor laser have considered only a single-laser pulse and discharge pulse, and as a result have had to assume initial conditions [5]–[8]. This approach has difficulty in accurately modeling laser properties as a function of charging voltage, capacitance, repetition rate, and tube temperature since a number of discharge pulses and interpulse relaxation periods are required before consistent, reproducible initial conditions are obtained.

In a previous paper [9], we reported an analysis of the copper chloride double pulse laser in which a dissociation discharge pulse was modeled and the results were used as initial conditions for an analysis of the pumping discharge pulse. In this way, laser pulse energy as a function of the time delay between discharge pulses could be calculated. In this paper, we report a similar analysis for the high repetition rate pure copper laser. Coupled rate equations describing the time rate of change of the number density of selected atomic levels of copper and helium (the buffer gas) as well as laser intensity, electron density, electron temperature, gas temperature and discharge current, and voltage were formulated. Initial conditions were assumed. The equations were integrated, simulating the discharge pulse and interpulse afterglow period. After a time τ had elapsed representing one cycle [$\tau = (\text{repetition rate})^{-1}$], the densities and temperatures were compared to the initial conditions. If a given convergence was not achieved, the laser was pulsed again and the process repeated. In this way, a consistent laser pulse, discharge pulse, number densities, and temperatures were computed for an entire cycle.

In an ideal HRR copper vapor laser, quantities such as charging voltage, capacitance, metal density, and repetition rate are independent and can be uniquely specified. In an ideal laser, one is able to specify thermodynamic quantities, access any tube temperature, and uniformly deposit energy throughout the active volume. The discharge circuit of an ideal laser is free of inductance. In a real HRR laser, the tube temperature and metal density are functions of the discharge input power so that the charging voltage, capacitance, repetition rate, and metal density are not independent. The buffer gas pressure can be specified exterior to the tube but cannot be accurately known within the tube due to transient discharge heating. The materials used in the construction of real lasers set an upper limit on the tube temperature, and inductance in the discharge circuit limits the rate at which current and voltage appear across the tube. These limitations mask the physical processes which occur in a real HRR laser and make it difficult to deconvolve the effect of changing a single variable. Therefore, our analysis is divided into two sections. The first section

Manuscript received December 5, 1980; revised March 30, 1981. This work was supported by the U.S. Department of Energy.

The author was with Sandia National Laboratories, Albuquerque, NM 87185. He is now with the Lawrence Livermore National Laboratory, Livermore, CA 94550.

deals with the modeling of an ideal laser and clearly illustrates some of the basic physical processes taking place. Equipped with results from the ideal analysis, the second section examines and models the real laser, now better able to explain the computed and experimental results.

For the purpose of comparing the model to experimental data, conditions which simulate the VENUS copper were chosen. The VENUS laser is a 15 W device operating at about 6 kHz. The discharge tube is made of alumina with a 2.54 cm ID and a heated region 50 cm long. The laser has been described in detail elsewhere [4].

The results of the model indicate that the dependence of laser power on metal density (tube temperature) is primarily a function of the peak electron temperature. Since the peak electron temperature is a function of the peak voltage across the discharge tube, this value largely determines the optimum tube temperature and maximum laser power. The results also show that the dependence of laser power on repetition rate is a function of the initial metastable density, and that this value is a function of the dominant mode of relaxation (electron collision or diffusion).

We will discuss some details of the model in Section II. Characteristics of the ideal laser as a function of tube temperature, charging voltage, discharge capacitance, and repetition rate as computed with the model will be discussed in Section III. A comparison between computed and experimental results for a real laser will be made in Section IV. Conclusions and recommendations are contained in Section V.

II. DESCRIPTION OF THE MODEL

The model simulates a discharge pulse, laser pulse, and inter-pulse afterglow in a high repetition rate copper laser. Initial conditions are chosen and a number of cycles are computed until consistent pulses are obtained. The following species are considered in the model:

n_e	electrons
Cu	2S ground state copper
Cu_m	2D metastable copper (lower laser level)
Cu^*	2P copper (upper laser level)
Cu^{**}	lumped radiative state in copper
Cu^+	atomic copper ion
He	ground state helium
He_m	metastable state helium
He^*	lumped radiative state in helium
He^+	atomic helium ion
He_2^+	molecular helium ion
T_e	electron temperature
T_g	gas temperature
P_g	buffer gas pressure
P_{Cu}	copper vapor pressure
I_i, V_i	discharge current and voltage for circuit elements i
\mathcal{I}	laser intensity.

The helium metastable state is nominally the 2^3S level. For both helium and copper, we have included a lumped radiative state (He^* , Cu^{**}). These states act as a buffer for recombining ions. When an electron and ion recombine, the resulting atom is usually in an excited state. In our model, this state is He^* or Cu^{**} . Subsequent processes involving these states (e.g., spon-

taneous emission, electron excitation or relaxation) then determine what distribution of excited states results from electron-ion recombinations. This is especially important in the case of copper. If electron-ion recombinations preferentially populate the metastable 2D lower laser level, then pumping requirements to reach threshold are increased for the next laser pulse.

We have included the thermodynamic quantities T_g , P_{Cu} , and P_g . During the operation of a VENUS laser, the temperature of the discharge tube, which determines the copper vapor pressure, can be measured by an optical pyrometer. The buffer gas pressure is measured external to the laser tube. The temperature of the discharge tube remains essentially constant, as does the external buffer gas pressure; however, the gas temperature within the tube can change by many hundreds of degrees during the discharge pulse. An increase in gas temperature increases the local gas pressures P_g and P_{Cu} at the same rate. However, the relaxation of P_g and P_{Cu} proceeds at different rates. The equilibrium vapor pressure for P_{Cu} is that pressure determined by the wall temperature. Therefore, exclusive of changes in the gas temperature, the time constant for relaxation of P_{Cu} to its equilibrium value is Λ/v_d where Λ is the radial diffusion length of the discharge tube and v_d is the speed at which copper atoms diffuse to the wall. Similarly, the equilibrium pressure for the buffer gas is that pressure measured external to the tube. Therefore, exclusive of changes in the gas temperature, the time constant for relaxation of P_g to its equilibrium value is $l/2v_s$ where l is the length of the discharge tube and v_s is the sound speed. The gas temperature relaxes to the wall temperature with a time constant proportional to the radius of the discharge tube. With these assumptions, the time rate of change of P_g and P_{Cu} is

$$\frac{dP_g}{dt} = \frac{dT_g}{dt} \frac{P_g}{T_g} - (P_g - P_{ex}) \frac{2v_s}{l} \quad (1)$$

$$\frac{dP_{Cu}}{dt} = \frac{dT_g}{dt} \frac{P_{Cu}}{T_g} - (P_{Cu} - P_{vp}) \frac{v_d}{R} \quad (2)$$

where P_{ex} is the external buffer gas pressure and P_{vp} is the copper vapor pressure based on the wall temperature. It is assumed that both P_{ex} and P_{Cu} are constant. Assuming the gas density stays in equilibrium with the local temperature and pressure, the change in gas density due to changes in temperature and pressure can be written as

$$\frac{\partial n_g}{\partial t} = -\frac{n_g}{T_g} \frac{dT_g}{dt} + \frac{n_g}{P_g} \frac{dP_g}{dt} = -(P_g - P_{ex}) \frac{n_g 2v_s}{lP_g} \quad (3)$$

$$\frac{\partial n_{Cu}}{\partial t} = -\frac{n_{Cu}}{T_g} \frac{dT_g}{dt} + \frac{n_{Cu}}{P_{Cu}} \frac{dP_{Cu}}{dt} = -(P_{Cu} - P_{vp}) \frac{n_{Cu} v_d}{\Lambda P_{Cu}} \quad (4)$$

where n_g and n_{Cu} are the densities of the buffer gas and copper atoms.

The voltage across the laser tube, and current through laser tube are not only a function of the plasma impedance but depend on the particulars of the discharge circuit. Therefore, a detailed description of the discharge circuitry was included as part of the model. Different discharge circuits were used for the ideal and real lasers.

The ideal laser discharge circuit consists of a capacitor ini-

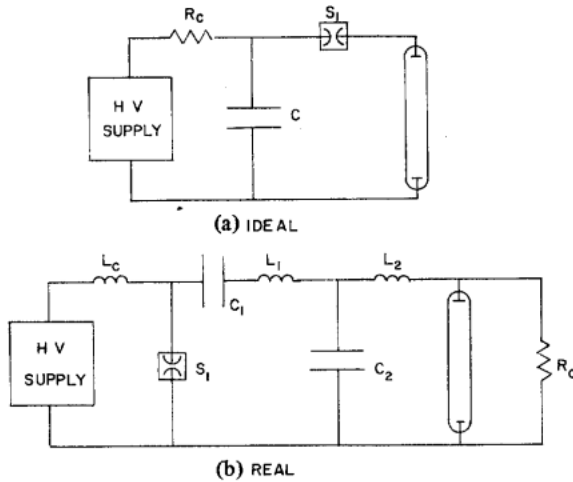


Fig. 1. Discharge circuits used in the model for (a) the ideal laser and (b) the real laser.

tially charged to a voltage V_0 , a thyatron with a switching time τ_s , and the discharge tube (see Fig. 1). The time rate of change of voltage across the tube is

$$\frac{dV}{dt} = f(\tau_s) V_0 - \frac{V}{R_d C} \quad (5)$$

where $f(\tau_s)$ is the voltage turn on function and R_d is the instantaneous discharge impedance

$$R_d = \frac{lm_e \nu}{n_e A e^2} \quad (6)$$

where m_e is the mass of the electron, ν is the electron collision frequency, and A is the effective cross-sectional area of the discharge tube.

The discharge circuit for the real laser simulates the actual circuit used for the VENUS laser. The details of the circuitry can be found elsewhere, and therefore are only briefly discussed here [1], [8]. The model discharge circuit is shown in Fig. 1. Capacitor C_1 is the storage capacitor resonantly charged to voltage V_0 by a dc power supply and inductance L_c . C_2 is a peaking capacitor. S_1 represents the thyatron switch and is modeled by a reverse bias voltage which is removed with a switching time τ_s . The parallel charging resistance is R_c . The thyatron is treated as a diode with current flowing through it in only one direction. The inductances L_1 and L_2 represent lumped circuit values. The differential equations describing the circuitry are

$$\frac{dI_1}{dt} = \frac{(V_1 - V_2 + V_0 f(\tau_s))}{L_1} \quad (7)$$

$$\frac{dI_2}{dt} = \frac{(V_2 - V_d)}{L_2} \quad (8)$$

$$\frac{dV_1}{dt} = -\frac{I_1}{C_1} \quad (9)$$

$$\frac{dV_2}{dt} = \frac{I_1 - I_2}{C_2} \quad (10)$$

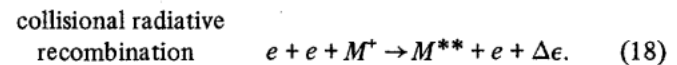
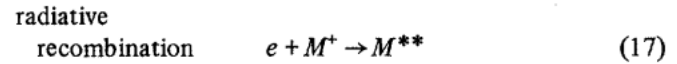
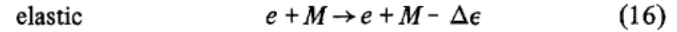
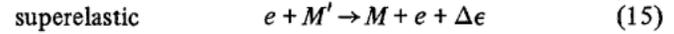
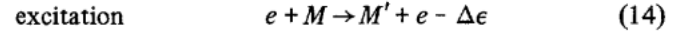
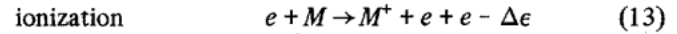
where current I_i flows through L_i and V_i is the voltage across capacitor C_i . The voltage across the discharge tube is

$$V_d = I_2 R_c R_d / (R_c + R_d) \quad (11)$$

while the current through the discharge tube is

$$I_d = I_2 R_c / (R_c + R_d). \quad (12)$$

The kinetic model includes two classes of collisions: electron-atom and atom-atom. The following electron impact reactions were included:



M represents all states of either copper or helium. M' is a state higher than M for the particular reaction. M^{**} is the highest radiative state. The $\Delta\epsilon$ represents a contribution to the change in electron energy.

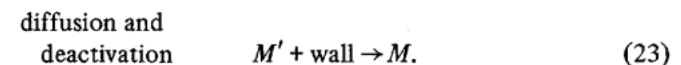
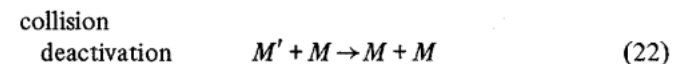
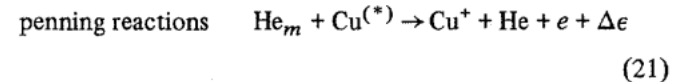
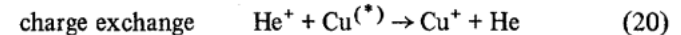
Ionization out of all levels was included, as well as excitation and superelastic relaxation between all applicable levels. Although the lower laser level is metastable and its excitation cross section is small compared to the upper level, its threshold energy is 1.39 eV as compared to 3.82 eV for the upper laser level. Therefore, at low electron temperatures, the excitation rate to the lower laser level can exceed the excitation rate to the upper laser level. This sets severe limits on pumping requirements and ultimately determines the optimum metal density.

Electron diffusion is ambipolar whose rate is

$$R_D = \frac{n_e M^+ (D_e \mu^+ + D^+ \mu_e)}{\Lambda^2 (\mu_e n_e + \mu^+ M^+)} \quad (19)$$

where D and μ are the individual diffusion coefficients and mobilities, and Λ is the diffusion length.

The major atom-atom collisions are between excited helium states and neutral copper. The atom-atom collisions included are



The charge exchange and Penning reactions are sufficiently fast so that copper ions are the only positive charge carriers after tens of microseconds following the discharge pulse. Superelastic collisions and diffusion are the major quenching mechanisms for the lower laser level. Since the superelastic relaxation rate is a function of the electron temperature and density, while the thermal diffusion relaxation rate is nearly

constant, the particular afterglow conditions determine which of these two methods is the most important. Conditions which favor the less efficient diffusion process are detrimental to the performance of the laser. We will see that since the initial metastable density is responsible for setting the threshold requirements, the particular mode of relaxation which dominates is one of the major factors which limits the lasers performance.

The electron distribution function is assumed to be Maxwellian. Since many iterations and integrations of stiff equations are required, the assumption was made for reasons of economy. In reality, as the metal density increases, the electron distribution function becomes depleted in electrons with energy greater than the copper threshold values. The Maxwellian assumption therefore yields rates which favor high threshold events at the expense of low threshold events. The net result is that excitation and ionization of the helium buffer is probably overestimated by a Maxwellian distribution, as is excitation of the upper laser level with respect to the lower laser level. During the afterglow period, the characteristic electron energy is below the threshold values for excitation. A Maxwellian distribution is therefore probably a good approximation during the afterglow. The time rate of change of the electron temperature can be written as

$$\begin{aligned} \frac{3}{2} k \frac{dT_e}{dt} = & \frac{e^2 E^2}{m_e \nu} + \sum_{i,j} \frac{He_m N_{ij} r_{ij}^P \Delta \epsilon_{ij}^P}{n_e} + \sum_{i,j < k} \\ & \cdot N_{ij} r_{ikj}^s \Delta \epsilon_{ikj}^s - \sum_{i,j > k} N_{ik} r_{ijk} \Delta \epsilon_{ikj}^P \\ & - \frac{3}{2} \frac{D_a}{\Lambda^2 n_e} k T_e - \sum_{i,j} N_{ij} r_{ij}^I \frac{3}{2} k T_e \\ & - \frac{3}{2} k (T_e - T_g) \sum_{ij} N_{ij} r_{ij}^e \frac{2m_e}{M_i}. \end{aligned} \quad (24)$$

The first three terms represent energy inputs to the electron distribution and the last four terms represent energy sinks. The first term is due to the applied electric field. The second term is due to Penning ionizations of species i , level j with rate constant r_{ij}^P injecting an electron of energy $\Delta \epsilon_{ij}^P$ into the distribution. The third term represents the increase in energy due to superelastic relaxation of species i between levels j and k separated by energy $\Delta \epsilon_{ijk}$. The next term is the energy loss due to excitations and ionizations followed by the energy loss due to diffusion (i.e., diffusion cooling). Secondary electrons are assumed to be born with zero energy and must be thermalized to the current electron temperature. This process occurs through electron-electron collisions which we assumed to be instantaneous. The reduction in average electron temperature due to this process is represented by the sixth term of (24), where r_{ij}^I is the ionization rate for species N_{ij} . The last term is the electron thermalization due to elastic collisions with species N_{ij} of temperature T_g and mass M_i at the rate r_{ij}^e . This term also includes Coulomb collisions with ions.

Rate equations for the electron density and for the density of the upper and lower laser levels are given as follows:

$$\begin{aligned} \frac{dn_e}{dt} = & n_e \left(\sum_{i,j} r_{ij}^I N_{ij} - \frac{D_a}{\Lambda^2} - \sum_i N_i^+ (r_{RR} + n_e r_{CRR}) \right) \\ & + He_m \sum_{i,j} r_{ij}^P N_{ij} \end{aligned} \quad (25)$$

$$\begin{aligned} \frac{d[Cu_m]}{dt} = & n_e (r_{12} [Cu] + r_{32}^s [Cu^*] + r_{42}^s [Cu^{**}] \\ & - (r_{21}^s + r_{23} + r_{24} + r_2^I) [Cu_m]) + \frac{Cu^*}{\tau_{32}} + \frac{Cu^{**}}{\tau_{42}} \\ & - \left(r_{21, Cu}^e [Cu] + r_{21, He}^e [He] - r^P [He_m] \right. \\ & \left. - r^{CE} [He^+] - \frac{D_{Cu}}{\Lambda^2} \right) [Cu_m] \\ & + \mathcal{B} \left([Cu^*] - \frac{g_3}{g_2} [Cu_m] \right) \end{aligned} \quad (26)$$

$$\begin{aligned} \frac{d[Cu^*]}{dt} = & n_e (r_{13} [Cu] + r_{23} [Cu_m] + r_{43}^s [Cu^{**}] \\ & - (r_{31}^s + r_{32}^s + r_{34} + r_3^I) [Cu^*]) + \frac{Cu^{**}}{\tau_{43}} \\ & - \left(r_{32, Cu}^e [Cu] + r_{32, He}^e [He] - r^P [He_m] \right. \\ & \left. - r^{CE} [He^+] - \frac{D_{Cu}}{\Lambda^2} - \frac{1}{\tau_{32}} + \frac{1}{\tau_{31}} \right) [Cu^*] \\ & - \mathcal{B} \left([Cu^*] - \frac{g_3}{g_2} [Cu_m] \right). \end{aligned} \quad (27)$$

In (25), the first and second terms represent the increase in electron density due to ionization of species N_{ij} and the decrease in density due to diffusion and recombination at the walls. The third term is the loss of electrons due to recombination with ions of species N_i by radiative recombination (with rate r_{RR}) and collisional radiation recombination (with rate r_{CRR}). The last term is the increase in electron density due to Penning ionizations.

In the rate equations for the lower (Cu_m) and upper laser levels (Cu^*), the following notation is used. The electron impact rate for excitation of copper from state i to state j is r_{ij} where the superscript s signifies a superelastic collision. Ground state copper (Cu) is state 1, the lower laser level (Cu_m) is state 2, the upper laser level (Cu^*) is state 3, and the lumped radiative state (Cu^{**}), which is the product of electron-ion recombination, is state 4. Ionization of state i by electron impact has rate constant r_i^I and the rate of collisional deactivation of state i to state j by species N is $r_{ij, N}^e$. The rates of charge exchange and Penning ionization are r^{CE} and r^P , and τ_{ij} is the radiative lifetime (including trapping factors) for state i to state j . The rate of stimulated emission due to cavity intensity \mathcal{B} is B , and g_i is the statistical weight of level i . Note that a change in density for the excited states of copper as a result of a change in gas temperature and pressure does not appear in (26) and (27). This is due to the assumption that all excited

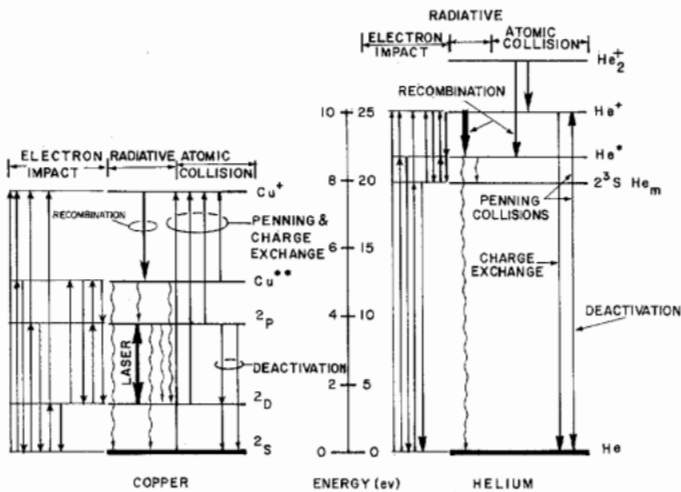


Fig. 2. A schematic representation of collisional and radiative processes included in the model.

states diffusing to the walls collisionally relax to the ground state. This relaxation proceeds with the rate constant D_{Cu}/Λ^2 .

The gas temperature is calculated by considering joule heating as a source during the current pulse and elastic collisions as a source during the afterglow. Conduction to the discharge tube wall, whose temperature is assumed to be constant, is the energy sink.

We have modeled the HRR copper laser primarily as a discharge and kinetics problem rather than an optics problem. Unlike other lasers where optical processes are dominant in determining the distribution of excited states, optical processes are of secondary importance in doing the same in the copper laser. As will be discussed later, electron impact processes dwarf stimulated emission in terms of populating and depopulating the laser levels. As a result, we have developed a simple optical model. The optical processes can be grouped into spontaneous and stimulated events.

Spontaneous emission from all radiative states to all lower states was included. Radiation trapping factors were calculated using the Holstein method for transitions terminating on the ground state [10]. Amplified spontaneous emission was included for the laser transition. We have considered only the 5106 Å transition in our analysis. The time rate of change in cavity intensity is therefore

$$\frac{dI}{dt} = h\nu c B I \left([Cu^*] - \frac{g_3}{g_2} [Cu_m] \right) l_a/l_c - cI ((1-R)/l_c + \gamma) + h\nu c A [Cu^*] \alpha. \quad (28)$$

The first term of (28) is for stimulated emission and absorption. l_a is the length of the heated region and l_c is the length of the optical cavity. The second term represents losses due to output coupling with mirror reflectivity R and distributed losses γ . The last term is a spontaneous emission startup term where A is the Einstein coefficient, $[Cu^*]$ is the density of the upper level, and α is a geometrical factor. The optical transitions described above, as well as the major kinetic processes included in the model, are illustrated in Fig. 2.

Most of the pertinent rate constants are discussed in detail in

[9]. The form of the rate equations which result from the processes discussed above can also be found in [9].

Rates for electron impact events were obtained by averaging the energy dependent cross section over a Maxwellian distribution. The electron impact cross sections for helium were obtained from the compilation by Kieffer [11]. Momentum transfer and electron impact cross sections for the excitation of the laser levels were obtained from the experimental data of Trajmar *et al.* [12] using the renormalization given by Hazi and Winters [13]. The renormalization increases the cross section for excitation of the lower level by a factor of three from that value given by Trajmar. Electron impact rates for the ionization of ground state copper, ionization out of excited states, and transfer between excited states were taken from [14]. Superelastic collision rates were computed from the excitation rates using the principle of detailed balance [15].

The lowest energy for which Trajmar *et al.* lists a cross for electron impact excitation of copper is 6 eV [12]. The cross section was extrapolated to zero at the threshold energy of the transition. Since the ratio of excitation of the 2D state to the 2P state as a function of electron temperature in the range of 2–6 eV is an important parameter (see discussion below), the energy dependence of the excitation cross sections of the 2D and 2P states at low electron energy are especially important. The lack of experimental data in the electron energy range less than 6 eV therefore is a limiting factor in the accuracy of the model.

For the results discussed in Section IV, the conductivity of the discharge tube was increased by a factor of five from what one would calculate from the electron collision frequency. This factor was found necessary in order for the maximum value of the calculated discharge current to match the experimental value. Apart from the mentioned normalization, there are no adjustable parameters in the model.

For reasonable initial conditions, about four iterations (i.e., discharge cycles) are required for the solution to converge to its steady state value.

III. THE IDEAL LASER

In development of the model, the greatest emphasis was placed on kinetic processes rather than optical processes. The degree to which kinetic processes dominate the populating and quenching mechanisms for the upper 2P and lower 2D laser levels is shown in Fig. 3. Here we have summed the total number of events which contribute to changing the population of the laser levels during one cycle. Electron impact excitation and superelastic relaxation between the ground state and the laser levels, as well as between the laser levels, dominate the populating and quenching events. Transitions between the laser levels due to laser emission are less important by more than two orders of magnitude. When laser emission is suppressed in the model, the change in the populations of the laser levels is very small.

Many of the results which follow can be explained with the aid of Fig. 4. Here we see the excitation rate from the ground state to the 2D state normalized by the rate from the ground

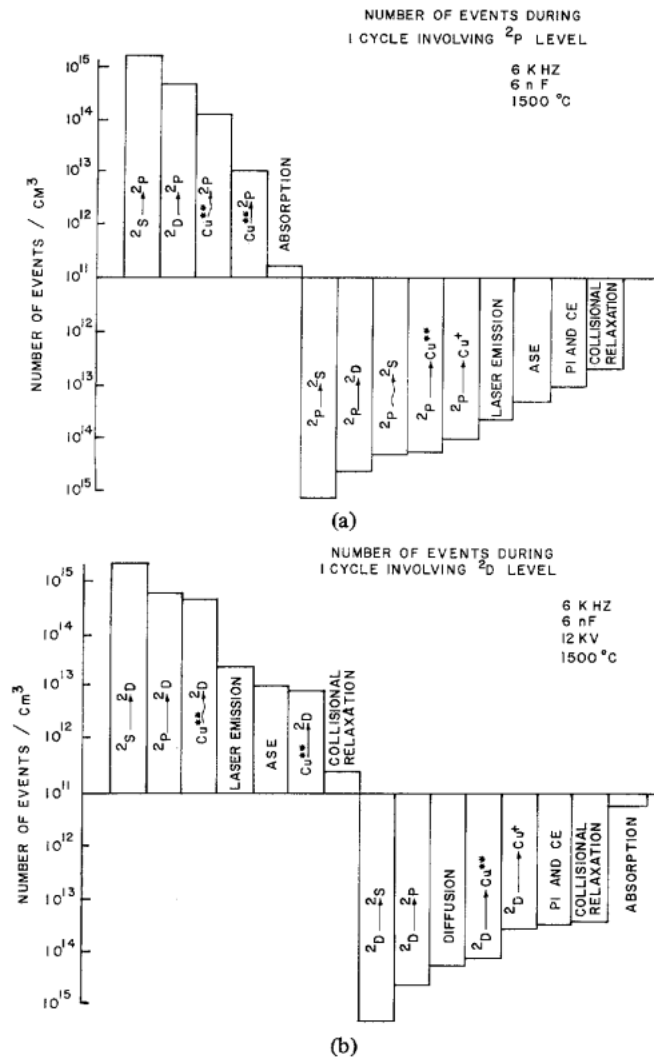


Fig. 3. The sum of the number of events involving the laser levels during one cycle. Bars above the midline represent populating events while bars below the midline represent quenching events. Straight arrows represent electron impact events, curved arrows represent radiative processes, PI is Penning ionization, CE is charge exchange, and ASE is amplified spontaneous emission. (a) $2P$ level and (b) $2D$ level.

state to the $2P$ level; and the excitation rate from the ground state to states higher than the $2P$ normalized by the rate to the $2P$ level. Clearly, there is an optimum electron temperature below which excitation of the lower level becomes increasingly important and above which the probability for excitation to higher lying states begins to dominate. Since at the beginning of the discharge pulse in a HRR laser there is usually a significant density of copper atoms in the lower level, peak electron temperatures which fail to exceed about 4 eV have difficulty reaching threshold. Similarly, peak electron temperatures which exceed 10 or 11 eV are not efficiently exciting the upper level and laser power decreases.

Laser power as a function of tube temperature for various charging voltages is shown in Fig. 5. All other parameters ($P_g = 9$ torr, rep. rate = 6 kHz, $C = 6$ nF) are fixed. (The copper density based on tube temperature in degrees centigrade is $1.23 \times 10^7 \exp(0.0124 T_w)/\text{cm}^3$ [18]. A tube temperature of 1450°C corresponds to a density of $7.53 \times 10^{14}/\text{cm}^3$.) We have computed minimum, optimum, and maximum tube

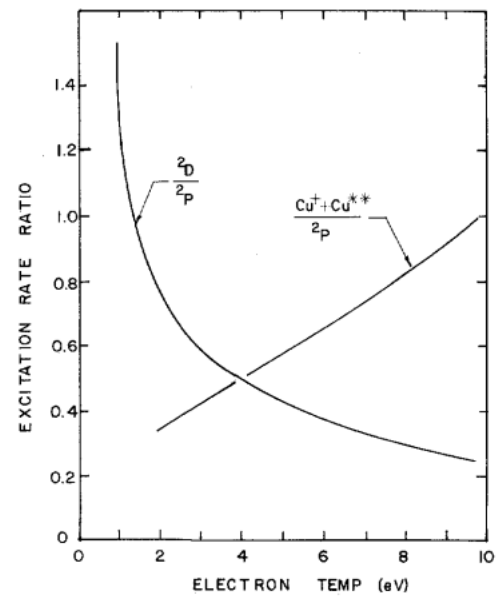


Fig. 4. The ratio of excitation rates from the ground state to the $2D$, $2P$, Cu^+ , and Cu^{**} states as a function of electron temperature.

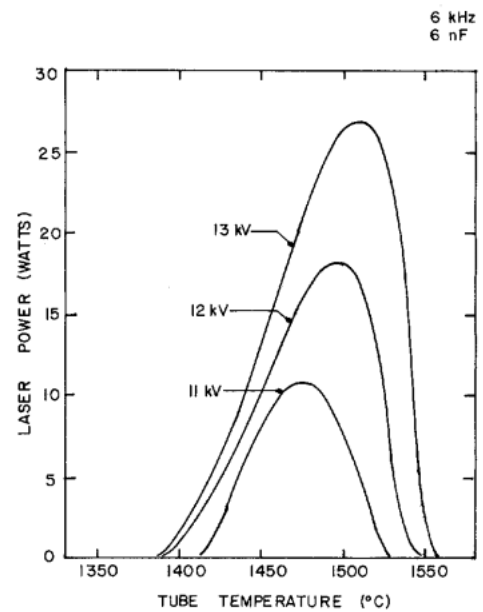


Fig. 5. Laser power as a function of tube temperature (copper vapor pressure) and charging voltage (V_0) for the ideal laser. The repetition rate is 6 kHz and circuit capacitance is 6 nF.

temperatures displaying behavior which has been observed experimentally [16]. We have also reproduced the experimentally observed increase in optimum tube temperature as the charging voltage is increased [16] (see Fig. 6). The increase in laser power between the minimum and optimum tube temperature is a result of the increase in copper density. The decrease in laser power and its eventual cutoff can be explained by the dependence of the electron temperature on metal density (see Fig. 7). As the copper density increases, the peak electron temperature decreases. This is due to the large momentum transfer cross section for copper as compared to helium. For a given charging voltage, the electron temperature eventually decreases to a small enough value so that the rate of excitation to the lower laser level becomes comparable to that

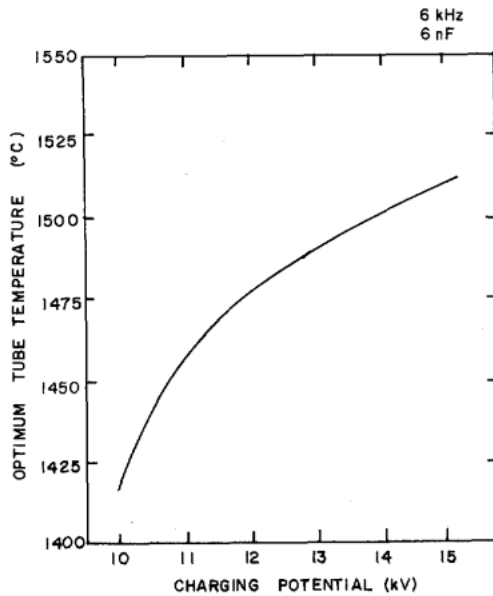


Fig. 6. Optimum tube temperature as a function of charging voltage.

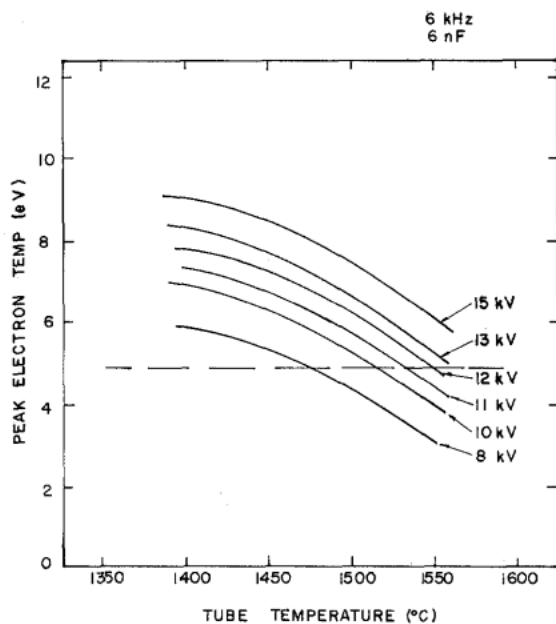


Fig. 7. The peak electron temperature as a function of tube temperature for various charging voltages V_0 . The horizontal line represents a minimum electron temperature below which threshold will not be reached under most conditions.

of the upper laser level and laser power decreases. Finally, at a sufficiently high metal density, excitation of the lower level dominates and laser oscillation cannot be sustained. The decrease in electron temperature lowers the overall excitation and ionization rate so that the electron density also decreases. Since superelastic relaxation of the metastable lower laser level is the preferred deexcitation mechanism (as compared to diffusion and relaxation at the walls), metastable atoms are not only being excited at a larger rate but are being relaxed at a slower rate as the tube temperature increases.

The increase in optimum tube temperature with increasing charging voltage is due to the same basic mechanism as described previously. Let us define a critical electron temperature

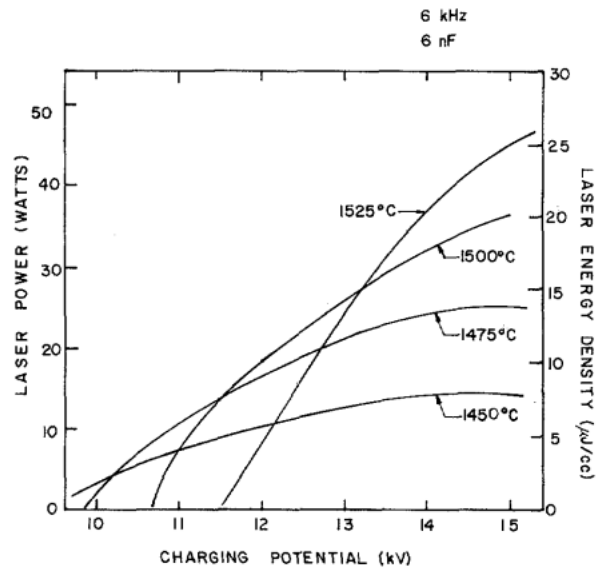


Fig. 8. Laser power as a function of charging voltage for various tube temperatures. The rate of change in laser power increases as the metal density increases.

T_e below which, for otherwise constant conditions, laser power decreases. To first order, $T_{e,max} \sim V_0/\ln T_w$ where V_0 is the charging voltage and T_w is the wall temperature. If T_e' corresponds to some value of V_0 and T_w , and V_0 is increased, then T_w and, hence, the metal density can be increased before $V_0/\ln T_w$ decreases to the critical value again. Therefore, the optimum tube temperature increases with increasing charging voltage.

By increasing the charging voltage and hence the optimum tube temperature, a larger fraction of the copper atoms contribute to the laser power. Therefore, the laser efficiency is also greater. This is more clearly seen in Fig. 8 where laser power as a function of charging voltage for given tube temperatures is plotted. (For similar experimental results, see [3] and [16]). For low tube temperatures, laser power saturates with respect to V_0 but for high tube temperatures, laser power increases almost linearly with V_0 . When T_w is increased, the threshold voltage is increased since a higher voltage is required to bring $V_0/\ln T_w$ above T_e' . The laser therefore operates inefficiently at low V_0 but quickly recovers until maximum efficiency is reached at large V_0 and T_w .

Fig. 9 shows the fraction of discharge energy expended during one cycle as a function of tube temperature. As the tube temperature increases, more energy is spent exciting copper atoms at the expense of helium atoms; however, the efficiency of that expenditure decreases. This is due to the decreasing electron temperature and is shown by the decrease in the ratio of the energy expended in exciting the 2P level divided by the energy expended exciting the 2D level. If we look at the same type of diagram (Fig. 10) for constant T_w as a function of V_0 , we see that as V_0 is increased, less energy is spent exciting copper and more energy is spent exciting helium. Despite the decrease in the fraction of total energy used to excite copper, the energy is used more efficiently. This is shown by the increase in the $^2P/^2D$ ratio. This is the opposite behavior than we observed in the previous example.

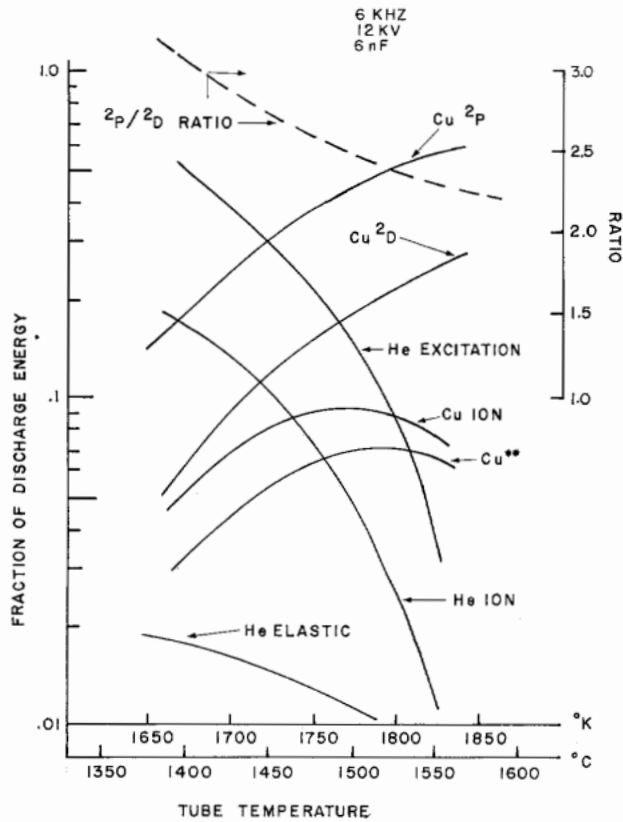


Fig. 9. The fraction of discharge energy expended in various excitation events and electron collisions as a function of tube temperature. As T_w increases, more energy is channeled into the copper, but the energy is used less efficiently.

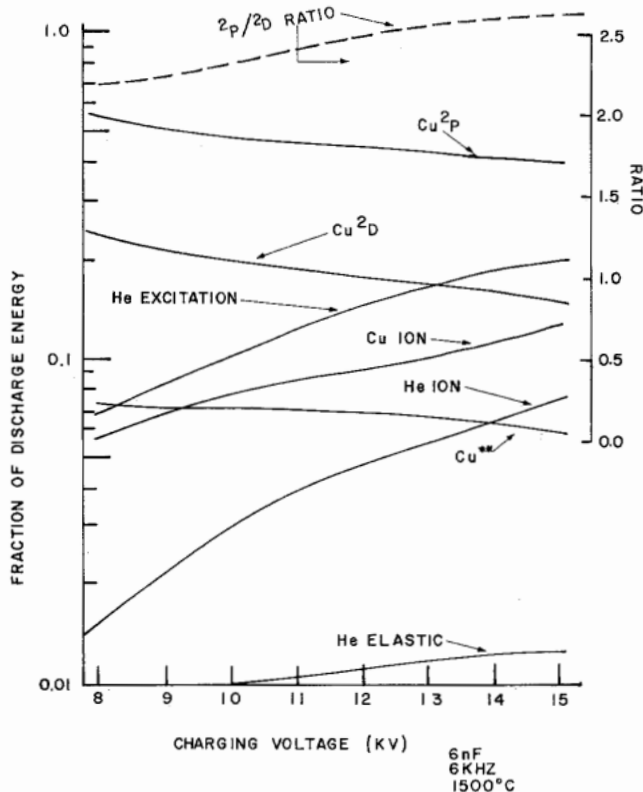


Fig. 10. The fraction of discharge energy expended in various excitation events and electron collisions as a function of V_0 . As V_0 increases, a smaller fraction of the energy is channeled into the copper but the energy is used more efficiently.

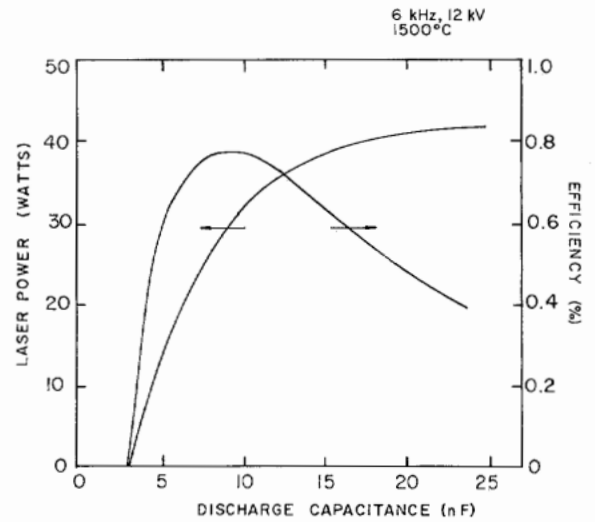


Fig. 11. Laser power and efficiency as a function of discharge capacitance for otherwise constant conditions.

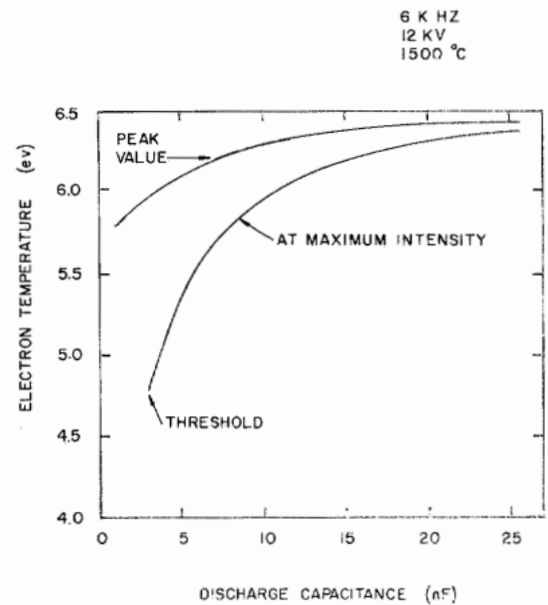


Fig. 12. The peak electron temperature during the discharge pulse and the electron temperature at peak laser intensity as a function of discharge capacitance. As these values become equal, laser power saturates with respect to capacitance.

We have just seen that for high metal densities, increasing input power by increasing charging voltage not only increases laser power but increases efficiency as well. The same is not true for increasing input power by increasing discharge capacitance (see Fig. 11). For constant tube temperature, laser power initially increases rapidly with increasing capacitance but soon saturates, reaching a maximum value. Laser efficiency is maximum at a smaller capacitance and lower power. This behavior is primarily due to two factors; the time dependent behavior of the electron temperature and the mode of relaxation of the lower laser level.

In a simple discharge circuit, $dV/dt = -V/RC$. Therefore, the larger the discharge capacitance, the longer a high voltage is sustained across the discharge tube. In Fig. 12 the peak electron temperature and the electron temperature at the maximum laser intensity for a 6 kHz laser are plotted as a function of discharge capacitance. With low discharge capacitance, the

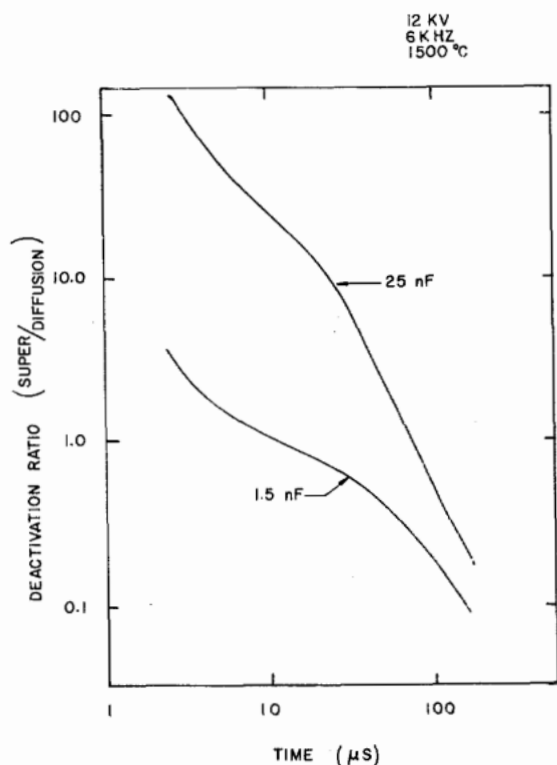


Fig. 13. The ratio of relaxation of 2D copper by superelastic electron collisions as compared to diffusion. The two cases represent a high average electron density and temperature (25 nF) and a low average electron density and temperature (2 nF).

electron temperature falls very quickly from its early peak value so that by the time the laser pulse appears, electron impact rates are unfavorable for continued excitation. As the capacitance is increased, the electron temperature stays near its peak value for a longer time so that electron impact rates remain favorable for a correspondingly longer period of time. This trend continues until the electron temperature at the maximum laser intensity is very nearly its peak value. Sustaining the electron temperature near its peak value beyond the time that the laser intensity is maximum by increasing capacitance nets a very small increase in laser power. This is due to the fact that the increasing metastable density has already reduced the laser gain to a small or negative value. At this point laser power saturates with respect to discharge capacitance. Increasing discharge capacitance further is a waste of energy which is reflected by the decrease in laser efficiency.

When the input power is increased by increasing capacitance, the average electron density during the interpulse period increases. This greatly affects the mode in which metastable copper atoms are relaxed. With large values of capacitance, relaxation by superelastic electron collisions are more important for a longer period of time than for small values of capacitance (see Fig. 13). Despite the fact that more metastable atoms are formed at the high input power levels, the relaxation rate is also larger so that the initial metastable density is largest for the smallest input powers. Hence, for otherwise constant conditions, large values of electron density during the interpulse period relax metastable atoms more efficiently and increase the laser extraction efficiency.

Laser power, pulse energy, and the initial metastable density

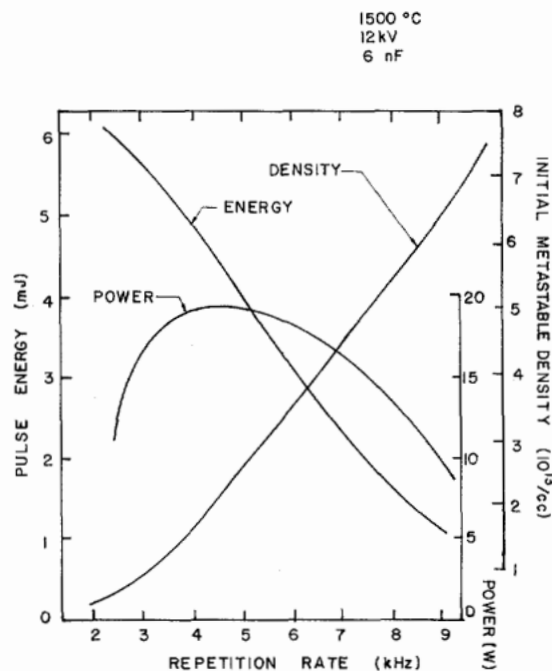


Fig. 14. Laser power, pulse energy, and initial metastable density as a function of repetition rate.

calculated as a function of repetition rate are shown in Fig. 14. The value of the initial metastable density dominates the performance of the copper laser as the repetition rate is increased. Laser pulse energy is usually largest for a single discharge pulse and decreases as the repetition rate increases since the initial metastable density increases as a result of the shorter relaxation time. (For similar experimental values, see [17].) Laser power increases with increasing repetition rate as long as the decrease in pulse energy is smaller than the increase in repetition frequency. For the ideal laser, and for otherwise constant conditions, laser pulse energy is inversely proportional to the initial metastable density, whose value is given by $n_{\max} \exp -1/\tau R$ where τ is the decay constant and R is the repetition rate. Laser pulse energy is proportional to the repetition rate. Hence, $P \sim R \exp 1/\tau R$, and the optimum repetition rate is $\approx 1/\tau$.

IV. THE REAL COPPER LASER

A typical current pulse and laser pulse, experimental and calculated, for the VENUS copper laser are shown in Fig. 15. The ringing in the circuit is between the discharge tube and peaking capacitor. The magnitude of ringing depends on the discharge impedance.

Since the tube temperature of a real HRR copper laser is a function of input power, the product $RCV^2/2$ must remain constant if the metal density is to remain constant during a given parametric study. One example is laser power as a function of repetition rate for constant metal density. For the experimental results of Fig. 16, the charging voltage was adjusted to keep the input power constant. Using the appropriate discharge circuit, the calculated results for the same conditions are shown in Fig. 17. In both examples, as the tube temperature and metal density increase, the optimum repetition rate decreases (see Fig. 18) and the dependence of laser power on repetition rate is more pronounced. Although the calculated

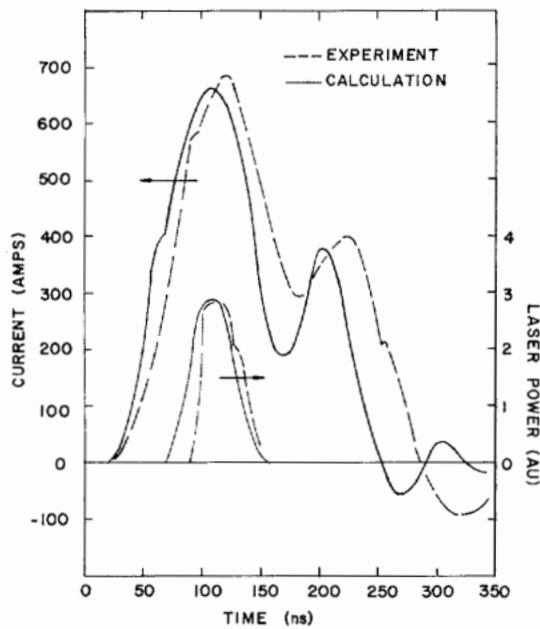


Fig. 15. Computed and experimental values of discharge current and laser power. The peak values of laser power have been normalized [19].

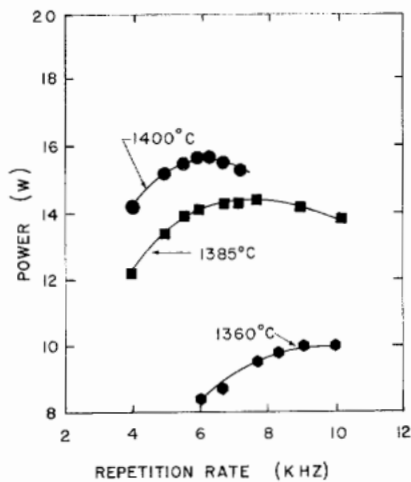


Fig. 16. Experimental values of laser power as a function of repetition rate for constant input power [19].

laser power is low, there is good agreement between the measured and calculated optimum repetition rates. With the results obtained from the analysis for the ideal laser, this behavior can now be explained.

We have already shown that in order to maximize laser pulse energy when the metal density has been increased, the charging voltage must also be increased. For constant input power, higher charging voltages are associated with lower repetition rates. Therefore, the optimum repetition rate decreases with increasing metal density. For a given charging voltage, the electron temperature decreases with increasing metal density. Therefore, for increasing and high repetition rates, the electron temperature falls more quickly for high metal densities than low metal densities. The decrease in laser power is therefore also more severe. The decrease in electron temperature also results in lower electron densities and higher initial metastable densities.

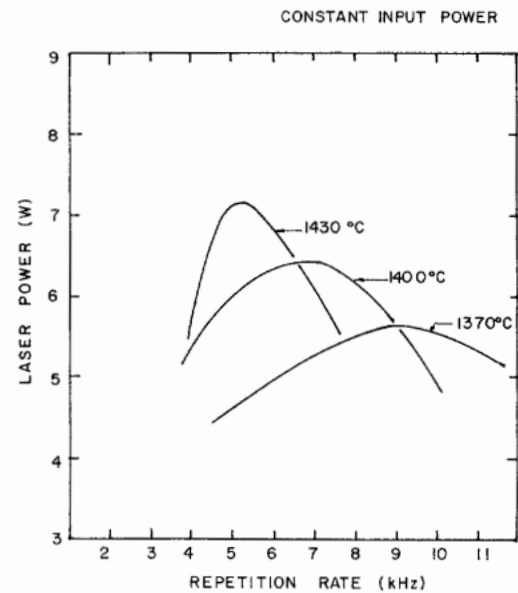


Fig. 17. Computed values of laser power as a function of repetition rate for constant input power.

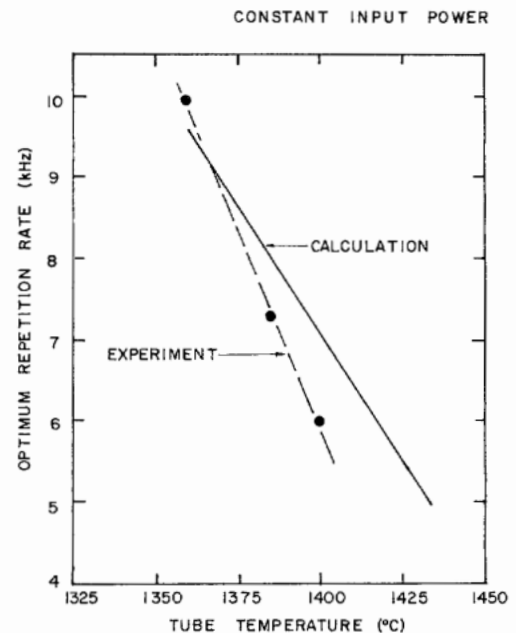


Fig. 18. The optimum repetition rate as a function of tube temperature for constant input power [19].

Laser power is also a function of buffer gas pressure, for which experimental and calculated results are shown in Fig. 19. (Input power remains constant for these examples.) The decrease in laser power with increasing buffer gas pressure is due primarily to the decrease in electron temperature. As the buffer gas pressure increases, the peak current decreases, but the current pulse length increases, both a result of the decreasing electron density. The initial metastable density also increases since the more efficient electron collision relaxation rate decreases with increasing pressure. At buffer gas pressures below optimum, excitation and ionization rates to states with thresholds greater than the 2P copper levels become increasingly more probable, especially those rates for exciting helium states. Despite the decrease in the density of ground state

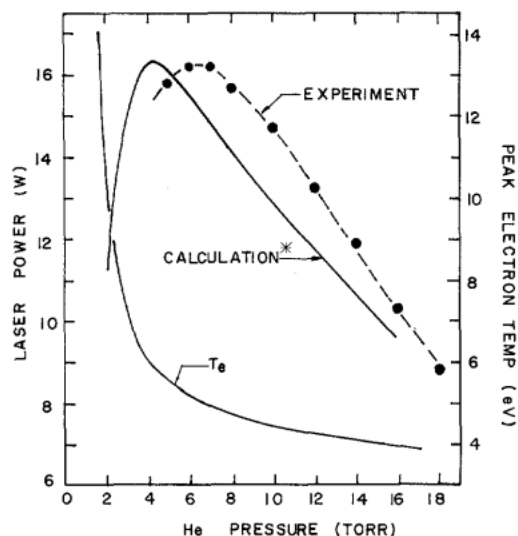


Fig. 19. Laser power and peak electron temperature (calculated) as a function of buffer gas pressure. The optimum laser powers have been normalized [19].

helium, the exponential increase in helium excitation rates yields a net increase in energy channeled into the buffer gas.

V. CONCLUDING REMARKS

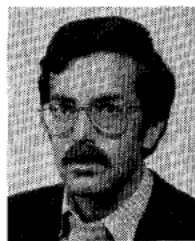
We have described and presented results for a model of a high repetition rate copper laser. This model differs from previously reported models in that initial conditions consistent with the discharge and laser parameters are obtained as part of the solution. We have found that the initial density of metastable copper and the peak electron temperature are the two major factors in determining laser power. Processes which directly effect these two quantities, such as the dominant mode of metastable relaxation, also affect laser power. Based on the analysis above, laser power can almost always be increased by increasing the charging voltage. Not only does increasing V_0 increase laser power at a given metal density, but it also increases the optimum tube temperature. The increase in optimum tube temperature could yield an exponential increase in laser power since the metal density increases exponentially with temperature. (For a given metal density, there is a voltage which will optimize laser power.) The upper limit to increasing laser power is currently set by the materials used in the construction of discharge tubes. The maximum material temperature sets an upper limit to the discharge input power and hence voltage. Due to this limitation, copper lasers and metal vapor lasers in general are operating far below their potential in both laser power and extraction efficiency.

ACKNOWLEDGMENT

The author would like to thank Dr. B. E. Warner of Lawrence Livermore National Laboratories for his comments and for graciously supplying experimental data for the VENUS laser. The author would also like to thank Dr. J. L. Miller of Lawrence Livermore National Laboratories whose preliminary work was used in modeling the real discharge circuit, and Dr. J. B. Moreno of Sandia National Laboratories for his review of the manuscript.

REFERENCES

- [1] R. S. Hargrove, R. Grove, and T. Kan, "Copper vapor laser resonator oscillator and oscillator-amplifier characteristics," *IEEE J. Quantum Electron.*, vol. QE-15, pp. 1228-1233, 1979.
- [2] I. Smilanski, A. Kerman, L. A. Levin, and G. Erez, "Scaling of the discharge heated copper vapor laser," *Opt. Commun.*, vol. 25, pp. 79-82, 1978.
- [3] P. A. Bokhan and V. A. Gerasimov, "Optimization of the excitation conditions in a copper vapor laser," *Sov. J. Quantum Electron.*, vol. 9, pp. 273-275; R. S. Anderson, B. E. Warner, C. Larson, Sr., and R. E. Grove, "100-W copper vapor laser oscillator," presented at CLEO-81, Washington, DC, 1981.
- [4] R. E. Grove, "The Venus copper laser system," in *Proc. Int. Conf. Lasers '79*, Orlando, FL, 1979.
- [5] K. G. Harstad, "Computer simulated rate processes in copper vapor lasers," *IEEE J. Quantum Electron.*, vol. QE-16, pp. 550-558, 1980.
- [6] G. M. Kull, N. Solimene, and W. T. Walter, "Modeling of pulsed gas lasers and comparison with experimental results for the copper vapor laser," in *Proc. Int. Conf. Lasers '79*, Orlando, FL, 1979.
- [7] P. A. Bokhan, V. A. Gerasimov, V. I. Solominov and V. B. Shcheglov, "Stimulated emission mechanism of a copper vapor laser," *Sov. J. Quantum Electron.*, vol. 8, pp. 1220-1227, 1978.
- [8] J. L. Miller, "Copper vapor laser kinetics model," Lawrence Livermore Lab. Rep. UC-18182, 1979.
- [9] M. J. Kushner and F.E.C. Culick, "A model for the dissociation pulse afterglow and laser pulse in the Cu/CuCl double pulse laser," *J. Appl. Phys.*, vol. 51, pp. 3020-3032, 1980.
- [10] T. Holstein, "Imprisonment of resonance radiation in gases II," *Phys. Rev.*, vol. 83, pp. 1159-1168, 1951.
- [11] L. J. Kieffer, "A compilation of electron collision cross section data for modeling gas discharge lasers," Joint Inst. Lab. Astrophys., 1973, Rep. NTIS COM-74-11661.
- [12] S. Trajmar, W. Williams, and S. K. Srivastava, "Electron-impact cross sections for Cu atoms," *J. Phys. B*, vol. 10, p. 3323, 1977.
- [13] A. U. Hazi, "Theoretical studies of electron collisions in electron transition lasers," presented at the 33rd Gaseous Electron. Conf., Norman, OK, 1980.
- [14] C. Deutsch, "Excitation and ionization of neutral atoms in a dense discharge," *J. Appl. Phys.*, vol. 44, p. 1142, 1973.
- [15] A.C.G. Mitchell and M. W. Zemansky, *Resonance Radiation and Excited Atoms*. New York: Cambridge Univ. Press, 1971, pp. 57-59.
- [16] P. A. Bokhan, V. I. Solomonov, and V. B. Shcheglov, "Investigation of the energy characteristics of a copper vapor laser with a longitudinal discharge," *Sov. J. Quantum Electron.*, vol. 7, pp. 1032-1033, 1977.
- [17] I. Smilanski, G. Erez, and L. A. Levin, "High power, high pressure, discharge heated copper vapor laser," *Opt. Commun.*, vol. 30, pp. 70-79, 1979.
- [18] A. N. Nesmeyanov, *Vapor Pressure of the Chemical Elements*. Amsterdam: Elsevier, 1963.
- [19] B. E. Warner, private communication, 1981.



M. J. Kushner was born in Los Angeles, CA, on December 21, 1952. He received the B.A. degree in astronomy and the B.S. degree in nuclear science from the University of California, Los Angeles, in 1976, and the M.S. and Ph.D. degrees in applied physics from the California Institute of Technology, Pasadena, in 1977 and 1979, respectively. His thesis was on metal halide double pulse lasers.

He was a Chaim Weissmann Postdoctoral Research Fellow at the California Institute of Technology. In January 1980 he joined the Analytical Spectroscopy Division of Sandia National Laboratories, Albuquerque, NM where his research included UV Raman spectroscopy in chemical vapor systems and studies of the plasma etching process. Since June 1, 1981 he has been with the Lawrence Livermore National Laboratory, Livermore, CA. He has published work on nuclear pumped plasmas and lasers, high repetition rate metal vapor lasers, and the CO chemical flame laser.